Cellular and Molecular Neurobiology (2019) 39:935–951
https://doi.org/10.1007/s10571-019-00689-1

ORIGINAL RESEARCH

Heterogeneity of GRIM-19 Expression in the Adult Mouse Brain

Sun-Nyoung Hwang[1] · Jae-Cheon Kim[1] · Seong Yun Kim[1]

Received: 21 December 2018 / Accepted: 14 May 2019 / Published online: 21 May 2019

Abstract
Gene associated with retinoid-interferon-induced mortality-19 (GRIM-19) is a subunit of the mitochondrial respiratory chain complex I that has a significant effect on ATP production. The brain is particularly susceptible to ATP deficiency due to its limited energy storage capability and its high rate of oxygen consumption. Thus, GRIM-19 might be involved in regulating ATP level in the brain or cell death caused by several neurological disorders. To understand the physiological and pathophysiological roles of GRIM-19 in the brain, a thorough investigation of the neuroanatomic distribution of GRIM-19 in the normal brain is necessary. Therefore, the present study examined the distribution patterns of GRIM-19 in the adult C57BL/6 mouse brain using immunohistochemistry and identified cell types expressing GRIM-19 using double immunofluorescence staining. We found that GRIM-19 was ubiquitously but not homogenously expressed throughout the brain. GRIM-19 immunoreactivity was predominantly observed in neurons, but not in astrocytes, microglia, or oligodendrocytes under normal physiological conditions. Following transient global cerebral ischemia, GRIM-19-positive immunoreactivity was, however, observed in neurons as well as glial cells including astrocytes in the hippocampus. Furthermore, GRIM-19 was weakly expressed in the hippocampal subgranular zone, in which neural stem and progenitor cells are abundant, but highly expressed in the immature and mature neuronal cells in the granular cell layer of the normal brain, suggesting an inverse correlation between expression of GRIM-19 and stemness activity. Collectively, our study demonstrating widespread and differential distribution of GRIM-19 in the adult mouse brain contributes to investigating the functional and pathophysiological roles of this protein.

Keywords Gene associated with retinoid-interferon-induced mortality-19 · Immunohistochemical distribution · Adult mouse brain · Mitochondrial respiratory chain complex I · Transient global cerebral ischemia

Introduction

Gene associated with retinoid-interferon-induced mortality-19 (GRIM-19) has been the subject of considerable interest because it affects several key cellular processes such as energy production, oxidative stress, and apoptosis (Angell et al. 2000; Fearnley et al. 2001; Huang et al. 2004; Lu and Cao 2008; Kalakonda et al. 2013). GRIM-19 is a critical component for assembly and function of the mitochondrial complex I (Huang et al. 2004) and maintenance of mitochondrial membrane potential (Lu and Cao 2008), which are required for ATP production via oxidative phosphorylation. Mitochondrial complex I is also known as the main site of reactive oxygen species (ROS) generation (Kushnareva et al. 2002). Indeed, there are several studies wherein downregulation of GRIM-19 resulted in increased ROS levels (Chen et al. 2012; Hu et al. 2017; Yang et al. 2018). On the other hand, the pro-apoptotic property of GRIM-19 has been intensively studied, especially in cancer research (Angell et al. 2000; Okamoto et al. 2010; Kalakonda et al. 2013). GRIM-19 was first identified by Angell et al. (2000), who showed that treatment of tumor cells with retinoic acid and interferon-β resulted in upregulation of GRIM-19 expression, followed by apoptosis (Angell et al. 2000). Several lines of evidence have confirmed its tumor-suppressive effect using genetic modification strategies (Angell et al. 2000; Okamoto et al. 2010; Kalakonda et al. 2013).

The brain is the most sensitive organ to ATP deprivation due to its limited energy storage and heavy requirement of ATP for normal functions (Lee et al. 2000). The brain is also vulnerable to ROS-mediated injury because this organ

✉ Seong Yun Kim
syk@catholic.ac.kr

[1] Department of Pharmacology, Department of Biomedicine & Health Sciences, Catholic Neuroscience Institute, College of Medicine, The Catholic University of Korea, 222 Banpo-daero, Seocho-gu, Seoul 06591, Republic of Korea

contains large amounts of iron and polyunsaturated fatty acids but relatively few antioxidants such as catalase (Halliwell 1989). Additionally, mounting evidence has confirmed that apoptosis is an important mechanism of many neurological disorders (Mattson et al. 2001). Taken together, these findings raise the possibility that GRIM-19 may be involved in the mechanism of neuronal cell death in the brain.

Indeed, several efforts have been made to determine the expression changes of GRIM-19 in brain tissue under pathological conditions. A significant reduction of GRIM-19 expression was observed in the substantia nigra neurons of Parkinson's disease patients (Grünewald et al. 2016) and in both the hippocampus and the motor cortex of aged rats (Tatarkova et al. 2016). Meanwhile, several reports on cerebral ischemia have shown a tendency of increased GRIM-19 expression in affected brain areas (Schneider et al. 2004; Mehrabian et al. 2007; Chomova et al. 2012). However, there has been no attempt to systematically study the expression patterns of GRIM-19 in the whole brain. Therefore, in the present study, we examined the neuroanatomic distribution of GRIM-19 immunoreactivity in the adult C57BL/6 mouse brain using immunohistochemistry. In addition, we performed double immunofluorescence staining in the hippocampus to identify the cell types expressing GRIM-19 under both normal and pathological conditions. Further, we showed double staining of GRIM-19 with various cellular markers representing distinct stages of adult neurogenesis in the subgranular zone (SGZ) of the hippocampus.

Materials and Methods

Animals

Male C57BL/6 mice (Orient Bio Inc., Seongnam, Korea) were housed under standard conditions (temperature 22 ± 1 °C, relative humidity 50 ± 3%, 12-h light–dark cycle, lights on at 08:00 am) with free access to food and water. A total of nineteen mice were used in this study: three mice (10 week old) for Western blot analysis to confirm antibody specificity, three mice (10 week old) for immunohistochemistry to examine the neuroanatomic distribution of GRIM-19 immunoreactivity in the normal mouse brain, three mice (10 week old) for double immunofluorescence staining to identify the cell types expressing GRIM-19 under normal conditions, and ten mice (11 week old) to investigate the effect of transient global cerebral ischemia on the expression pattern of GRIM-19. All animal procedures were approved by the Ethics Committee of the Catholic University of Korea and were performed in accordance with the National Institutes of Health's Guide for the Care and Use of Laboratory Animals (NIH Publication No. 80-23).

Transient Global Cerebral Ischemia

To induce transient global cerebral ischemia, mice were subjected to 40 min bilateral common carotid artery occlusion (BCCAO) followed by 3 days of reperfusion as described in literature with minor modifications (Cho et al. 2007). All surgeries were performed between 9 am to 5 pm. Briefly, anesthesia was induced with 2% isoflurane in 30% oxygen and 70% nitrous oxide for 3 min and maintained with 1.5% isoflurane in the same gas mixture. The body temperature was kept at 37.0 ± 0.5 °C. We measured regional cerebral blood flow (rCBF) using laser Doppler flowmetry (PF5010, Perimed, Järfälla, Sweden) to determine if brain ischemia was successfully induced. To do so, two flexible probes (407) were attached to the skull bilaterally 3.5 mm from bregma. rCBF was recorded by Perisoft, the Perimed analysis program (Perimed, Järfälla, Sweden), throughout the surgery. Then, both the common carotid arteries were isolated through a midline neck incision and clamped with micro-serrefines. Sham-operated animals underwent the same procedure except for occlusion of the common carotid arteries. The percentage of blood flow changes was calculated by dividing the average perfusion unit (PU) obtained during the 1 min immediately after occlusion by the baseline value and multiplying by 100. The hemispheres in which the percentage was more than 13% of the baseline were excluded in the analysis. After 40 min of occlusion, the micro-serrefines were removed and the skin was sutured. The animals were kept alive for 3 days in an incubator at 31 °C.

Tissue Collection

The animals were sacrificed at 10 am to avoid any variation due to circadian influences. Mice were killed under deep anesthesia with 15% chloral hydrate and transcardially perfused with 0.9% saline, followed by 4% paraformaldehyde in 0.1 M phosphate buffer (PB, pH 7.4). Brains were collected and post-fixed for 24 h at 4 °C in the same fixative. For cryoprotection, the fixed brains were incubated in 30% sucrose in 0.1 M PB for 2 days at 4 °C. The brains were embedded in Tissue-Tek OCT compound (Sakura Fine Technical, Tokyo, Japan) and flash-frozen using liquid nitrogen. The brains were stored at − 80 °C until use. Coronal brain Sections (20 μm thick) were collected from the olfactory bulb to the cerebellum with a cryostat and stored in phosphate-buffered saline (PBS, pH 7.4) with 0.04% sodium azide at 4 °C until use.

Confirmation of Antibody Specificity

The specificity of anti-GRIM-19 antibody used in this study was confirmed by Western blotting, as described previously (Choi et al. 2007). Ten micrograms of hippocampus homogenate were mixed with an equal volume of sample buffer and heated for 5 min at 95 °C. The proteins were analyzed by electrophoresis on 8 or 12% polyacrylamide gels for GRIM-19. Proteins were electrophoretically transferred from the SDS–polyacrylamide gel to nitrocellulose membrane (GE Healthcare, Amersham, UK). After being blocked with 5% bovine serum albumin (Affymetrix, Cleveland, OH, USA) for 1 h at room temperature (RT), the membrane was incubated with mouse anti-GRIM-19 antibody (1:2000, ab110240, Abcam, Cambridge, UK) overnight at 4 °C and then incubated with horseradish peroxidase-conjugated goat anti-mouse IgG antibody (1:2000, AP308P, Chemicon, Temecula, CA, USA) for 1 h at RT. Immunoreactive bands were visualized by enhanced chemiluminescent substrates (1896327, Pierce, Rockford, IL, USA). The Western blotting analysis confirmed the specificity of the antibody, which recognized one predominant band of approximately 16 kDa, corresponding to the reported size of GRIM-19 (Angell et al. 2000) (Fig. 1).

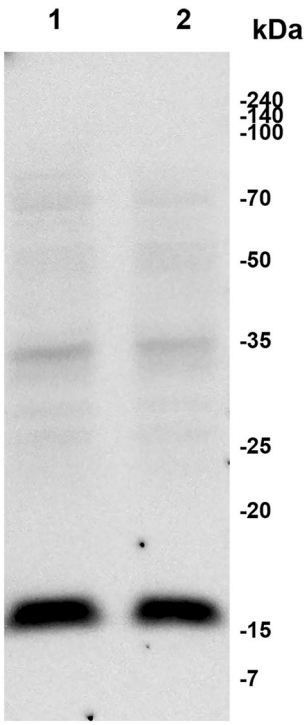

Fig. 1 Confirmation of antibody specificity for GRIM-19 in the hippocampus. The mouse monoclonal antibody against GRIM-19 detected a single predominant band with a molecular weight of approximately 16 kDa

Immunohistochemistry Staining

Free-floating sections were washed 3 times with 0.01 M PBS containing 0.05% Tween-20 (PBS-T) for 2 min each. Sections were blocked with 10% normal goat serum (NGS, S-1000, Vector Laboratories, Inc., Burlingame, CA, USA) in 0.01 M PBS for 1 h at RT and then blocked with unconjugated AffiniPure Fab fragment goat anti-mouse IgG (1:10, 115-007-003, Jackson ImmunoResearch Laboratories Inc., West Grove, PA, USA) in 0.01 M PBS for 1 h at RT before primary antibody application. Next, tissue slices were incubated with mouse monoclonal anti-GRIM-19 primary antibody (1:500, ab110240, Abcam, Cambridge, UK) overnight at 4 °C. On the following day, sections were incubated with biotinylated anti-mouse IgG (1:200, BA-2000, Vector Laboratories, Inc., Burlingame, CA, USA) for 2 h at RT and then in an avidin–biotin–peroxidase complex solution (1:50, PK-6100, Vector Laboratories, Inc., Burlingame, CA, USA) for 1 h at RT. Sections were then visualized with 0.1% diaminobenzidine tetrahydrochloride (DAB, D-5637, Sigma Chemical Company, St. Louis, MO, USA) and 0.005% H_2O_2 in 0.05 M Tris–HCl (TB, pH 7.4), and the reaction was terminated by several washes in TB. All tissue sections were scanned with Pannoramic Digital Slide Scanner (3DHistech Ltd., Budapest, Hungary), and the digital images were displayed with Pannoramic Viewer software (3DHistech Ltd., Budapest, Hungary). Sections were also examined with light microscopy (BX51, Olympus, Tokyo, Japan). The specificity of GRIM-19 immunoreactivity was confirmed by the absence of immunohistochemical reaction in sections from which the primary antibody was omitted, or in which it was substituted with non-specific mouse IgG.

Double Immunofluorescence Staining

For double immunofluorescence histochemistry, sections were washed with 0.01 M PBS-T 3 times for 2 min each. The sections were blocked with 10% NGS for 1 h at RT and then blocked with unconjugated AffiniPure Fab fragment goat anti-mouse IgG (1:10, 115-007-003, Jackson ImmunoResearch Laboratories Inc., West Grove, PA, USA) for 1 h at RT. Next, tissue slices were incubated with mouse anti-GRIM-19 primary antibody (1:500, ab110240, Abcam, Cambridge, UK) overnight at 4 °C. On the following day, the sections were incubated with Cy3-conjugated anti-mouse IgG (1:500, 715-165-151, Jackson ImmunoResearch Laboratories Inc., West Grove, PA, USA) for 2 h at RT. After being rinsed with 0.01 M PBS-T 3 times for 2 min each, the sections were blocked with 10% NGS for 1 h at RT and incubated overnight at 4 °C with one of the following antibodies: rabbit anti-neuronal nuclei (NeuN, 1:1000, ab177487, Abcam, Cambridge, UK), rabbit anti-glial fibrillary acidic protein (GFAP, 1:1000, AB5804, Millipore, Temecula,

CA, USA), rabbit anti-ionized calcium-binding adapter molecule 1 (Iba1, 1:300, 019-19741, Wako Pure Chemical Industries, Ltd., Osaka, Japan), rabbit anti-oligodendrocyte-specific protein (OSP, 1:1000, ab53041, Abcam, Cambridge, UK), rabbit anti-Ki-67 (1:1000, ab15580, Abcam, Cambridge, UK), guinea pig anti-doublecortin (DCX, 1:1000, AB2253, Millipore, Temecula, CA, USA), mouse anti-prospero-related homeobox protein 1 (Prox1, 1:500, MAB5654, Millipore, Temecula, CA, USA), mouse anti-polysialylated-neural cell adhesion molecule (PSA-NCAM, 1:200, MAB5324, Millipore, Temecula, CA, USA), mouse anti-Calretinin (1:500, MAB1568, Millipore, Temecula, CA, USA), or mouse anti-Calbindin (1:500, 214011, Synaptic Systems, Göttingen, Germany). On the third day, sections were incubated with the corresponding secondary antibodies for 2 h at RT: Alexa Fluor 488-conjugated anti-mouse IgG (1:500, A-11001, Thermo Fisher Scientific, Rockford, IL, USA), Alexa Fluor 488-conjugated anti-guinea pig IgG (1:500, A-11073, Thermo Fisher Scientific, Rockford, IL, USA), or Alexa Fluor 488-conjugated anti-rabbit IgG (1:500, A-11008, Thermo Fisher Scientific, Rockford, IL, USA). After a final rinse with 0.01 M PBS-T 3 times for 2 min each, the sections were mounted on a slide glass with Kaiser's glycerol gelatin (Merck, Germany) and coverslipped. The sections were then observed with a confocal microscope (LSM 510 Meta, Carl Zeiss Co., Ltd. Jena, Germany). The rate of colocalization of GRIM-19 with NeuN, GFAP, Iba1, OSP, Ki-67, DCX, Prox1, PSA-NCAM, Calretinin, or Calbindin in the hippocampal dentate gyrus was determined by Pearson's colocalization coefficient using Zen 2.1 SP1 software (Carl Zeiss Co., Ltd. Jena, Germany).

Histological Analysis

Sections were examined under a microscope at ×400 magnification to evaluate the expression of GRIM-19. Brain regions were identified using Allen Brain Atlas (www.brain-map.org), whose nomenclature was used in this study. The images underwent color deconvolution to separate hematoxylin (purple)- and DAB (brown)-stained color channels using IHC profiler plugin (Varghese et al. 2014) in ImageJ software (W. Rasband, National Institutes of Health, http://imagej.nih.gov/ij/). An appropriate threshold was chosen to select the positively stained area in the deconvoluted DAB images. Once a selection was made, the mean gray value and area of the defined region of interest were measured. The mean gray value was in the range from 0 to 255, where 0 and 255 represent black and white, respectively. GRIM-19 immunoreactivity was quantified by measuring the product of the intensity multiplied by the density, as described by Rizzardi et al. (2012). The intensity was calculated by subtracting the mean gray value from 255 and then divided by 255, where a value of 0 is equivalent to the

Table 1 Regional expression of GRIM-19 in the adult mouse brain

Region	Immunoreactivity
Cerebrum	
Olfactory areas	
Main olfactory bulb (MOB)	
Glomerular layer (gl)	25
Outer plexiform layer (opl)	25
Mitral layer (mi)	33
Granule layer (gr)	19
Accessory olfactory bulb (AOB)	25
Anterior olfactory nucleus (AON)	19
Piriform area (PIR)	29
Cerebral cortex (CTX)	
Layer 1	14
Layer 2/3	18
Layer 4	16
Layer 5	18
Layer 6	12
Hippocampal formation	
Hippocampus (HP)	
CA1	
Stratum oriens (so)	16
Pyramidal cell layer (py)	41
Stratum radiatum (sr)	15
CA2	
Stratum oriens (so)	20
Pyramidal cell layer (py)	39
Stratum radiatum (sr)	19
CA3	
Stratum oriens (so)	14
Pyramidal cell layer (py)	38
Stratum radiatum (sr)	15
Dentate gyrus (DG)	
Molecular layer (mo)	15
Granular cell layer (gr)	36
Polymorph layer (po)	21
Subiculum (SUB)	20
Amygdala	
Lateral amygdalar nucleus (LA)	17
Basolateral amygdalar nucleus (BLA)	18
Basomedial amygdalar nucleus (BMA)	13
Medial amygdalar nucleus (MEA)	16
Striatum	
Caudoputamen (CP)	15
Nucleus accumbens (ACB)	14
Olfactory tubercle (OT)	25
Lateral septal nucleus (LS)	9
Pallidum	
Globus pallidus (GP)	8
Substantia innominate (SI)	13
Medial septal nucleus (MS)	11

Table 1 (continued)

Region	Immunoreactivity
Diagonal band nucleus (NDB)	14
Bed nucleus of the stria terminalis (BST)	13
Interbrain	
Thalamus	
Anterodorsal nucleus (AD)	21
Anteroventral nucleus (AV)	17
Paraventricular nucleus (PVT)	11
Reticular nucleus (RT)	11
Nucleus of reuniens (RE)	10
Medial habenula (MH)	16
Lateral habenula (LH)	14
Lateral dorsal nucleus (LD)	17
Mediodorsal nucleus (MD)	11
Ventral posterior nucleus (VP)	16
Lateral geniculate complex (LG)	16
Medial geniculate complex (MG)	15
Hypothalamus	
Subfornical organ (SFO)	39
Lateral hypothalamic area (LHA)	8
Suprachiasmatic hypothalamic nucleus (SCH)	30
Retrochiasmatic hypothalamic area (RCH)	14
Dorsomedial hypothalamic nucleus (DMH)	11
Ventromedial hypothalamic nucleus (VMH)	10
Arcuate hypothalamic nucleus (ARH)	63
Midbrain (MB)	
Superior colliculus (SC)	7
Midbrain reticular nucleus (MRN)	6
Substantia nigra (SN)	
Reticular part (SNr)	10
Compact part (SNc)	11
Central linear nucleus raphe (CLI)	6
Inferior colliculus (IC)	8
Hindbrain	
Pons (P)	
Superior central nucleus raphe (CS)	7
Pontine reticular nucleus (PRN)	5
Tegmental reticular nucleus (TRN)	8
Pontine gray (PG)	9
Nucleus of the lateral lemniscus (NLL)	11
Principle sensory nucleus of the trigeminal (PSV)	12
Superior olivary complex (POR)	8
Parabrachial nucleus (PB)	9
Motor nucleus of trigeminal (V)	10
Medulla (MY)	
Nucleus prepositus (PRP)	6
Medial vestibular nucleus (MV)	6
Ventral cochlear nucleus (VCO)	16
Dorsal cochlear nucleus (DCO)	10
Gigantocellular reticular nucleus (GRN)	5
Parvicellular reticular nucleus (PARN)	6
Spinal nucleus of the trigeminal (SPV)	8
Paragigantocellular reticular nucleus (PGRN)	7
Cerebellum	
Cerebellar cortex (CBX)	
Molecular layer (mo)	12
Purkinje layer (Pk)	26
Granular layer (gr)	10
Cerebellar nuclei (CBN)	7
Fiber tracts	
Anterior commissure (aco)	1
Anterior forceps (fa)	2
Corpus callosum (cc)	1
Fimbria (fi)	5
Stria medullaris (sm)	0
Internal capsule (int)	2
Cerebral peduncle (cpd)	1
Optic tract (opt)	2
Dorsal hippocampal commissure (dhc)	1
Arbor vitae (arb)	1

The relative immunoreactivity of GRIM-19 is classified as: *absent* 0–4, *weak* 5–9, *moderate* 10–14, *strong* 15–19, *very strong* 20–29, *extremely strong* ≥ 30

lowest concentration of GRIM-19 proteins and 1 the highest. The density was expressed as the percentage of selected brain area versus total area. The immunoreactivity of GRIM-19, ranging from 0 to 100, was measured in various brain regions (Table 1). We classified GRIM-19 expression into five categories: immunoreactivity of 0–4 indicates absent (−); 5–9, weak (+); 10–14, moderate (++); 15–19, strong (+++); 20–29, very strong (++++); and ≥ 30, extremely strong (+++++).

Results

Regional Distribution of GRIM-19 Immunoreactivity

GRIM-19 showed ubiquitous, but not homogenous, distribution throughout the brain (Fig. 2). GRIM-19 immunoreactivity was markedly detected in the cell body around the nucleus (Fig. 7a–d). Overall, extremely strong staining of GRIM-19 was observed in the arcuate nucleus, subfornical organ, and suprachiasmatic nucleus of the hypothalamus, the pyramidal cell layer and granular cell layer of the hippocampus, and the mitral layer of the main olfactory bulb (MOB). GRIM-19 immunoreactivity was weakly detected in the globus pallidus, the lateral hypothalamic area, the

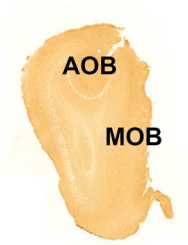

bregma 3.445 mm

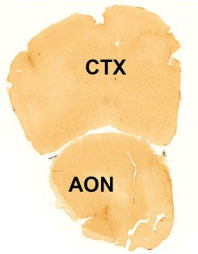

bregma 2.445 mm

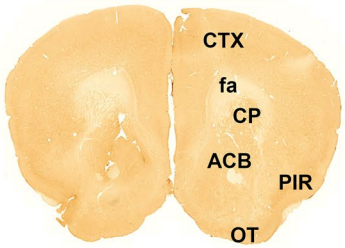

bregma 1.445 mm

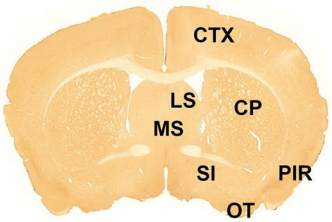

bregma 0.445 mm

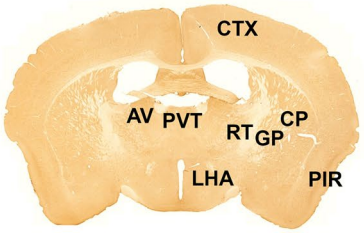

bregma -0.555 mm

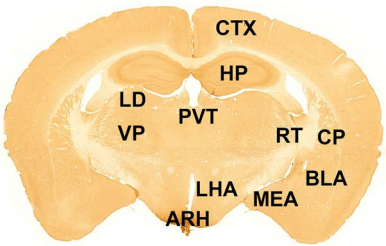

bregma -1.555 mm

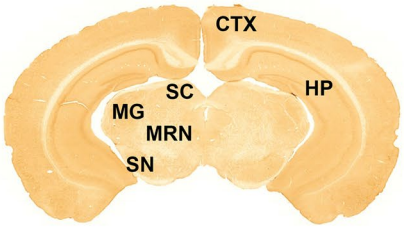

bregma -2.555 mm

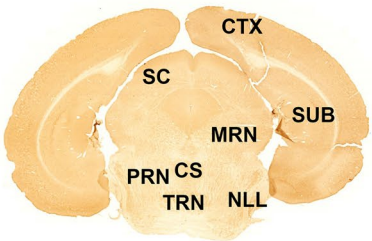

bregma -4.055 mm

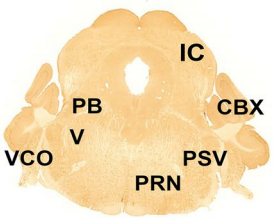

bregma -5.055 mm

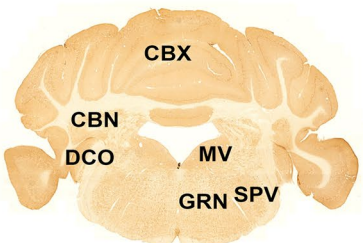

bregma -6.055 mm

◂**Fig. 2** GRIM-19 immunostaining in coronal sections of a C57BL/6 J mouse brain from the olfactory bulb to the cerebellum. *AOB* accessory olfactory bulb, *MOB* main olfactory bulb, *AON* anterior olfactory nucleus, *CTX* cerebral cortex, *CP* caudoputamen, *ACB* nucleus accumbens, *PIR* piriform cortex, *OT* olfactory tubercle, *fa* anterior forceps, *LS* lateral septal nucleus, *MS* medial septal nucleus, *SI* substantia innominate, *AV* anteroventral nucleus of the thalamus, *PVT* paraventricular nucleus of the thalamus, *RT* reticular nucleus of the thalamus, *GP* globus pallidus, *LHA* lateral hypothalamic area, *HP* hippocampus, *LD* lateral dorsal nucleus of the thalamus, *VP* ventral posterior complex of the thalamus, *ARH* arcuate hypothalamic nucleus, *BLA* basolateral amygdalar nucleus, *MEA* medial amygdalar nucleus, *SC* superior colliculus, *MG* medial geniculate complex, *MRN* midbrain reticular nucleus, *SN* substantia nigra, *CS* superior central nucleus raphe, *PRN* pontine reticular nucleus, *TRN* tegmental reticular nucleus, *NLL* nucleus of the lateral lemniscus, *SUB* subiculum, *IC* inferior colliculus, *PB* parabrachial nucleus, *V* motor nucleus of the trigeminal, *VCO* ventral cochlear nucleus, *PSV* principal sensory nucleus of the trigeminal, *CBX* cerebellar cortex, *CBN* cerebellar nuclei, *DCO* dorsal cochlear nucleus, *MV* medial vestibular nucleus, *GRN* gigantocellular reticular nucleus, *SPV* spinal nucleus of the trigeminal. *Scale bar*s indicate 1 mm

midbrain including the reticular nucleus and the central linear nucleus raphe, and the hindbrain including the superior central nucleus raphe, the pontine reticular nucleus, and gigantocellular reticular nucleus. There was no staining in the fiber tracts such as the corpus callosum, internal capsule, cerebral peduncle, optic tract, or arbor vitae. Quantitative analysis of GRIM-19 immunoreactivity is summarized in Table 1.

Olfactory Bulb

This region was intensely stained with the antibody to GRIM-19 (Fig. 3a). The granule layer of the MOB and anterior olfactory nucleus exhibited strong immunoreactivity. Stronger immunoreactivity was seen in the glomerular and outer plexiform layers of MOB, accessory olfactory bulb, and piriform cortex. The strongest staining was observed in the mitral layer of MOB.

Cerebral Cortex

Distinct expression patterns of GRIM-19 were found in the cerebral cortex (Fig. 3b). Moderate staining was observed in the molecular layer (layer 1) and polymorphic layer (layer 6), while strong immunoreactivity was seen in the external granular and pyramidal layers (layers 2/3), internal granular layer (layer 4), and internal pyramidal layer (layer 5).

Hippocampal Formation

GRIM-19 was expressed at moderate to strong levels in the stratum oriens and stratum radiatum of CA1-CA3 and molecular layer of the dentate gyrus (DG) (Fig. 3c). Stronger immunoreactivity of GRIM-19 was detected in the polymorph layer (hilar region) of the DG and subiculum. The strongest staining of GRIM-19 was observed in the pyramidal cell layers of CA1-CA3 and the granular cell layer of the DG.

Amygdala

Overall, moderate to strong staining of GRIM-19 was observed in the amygdala complex (Fig. 3d). The lateral amygdalar nucleus, basolateral amygdalar nucleus, and medial amygdalar nucleus showed strong immunoreactivity, while the basomedial amygdalar nucleus exhibited moderate GRIM-19 expression.

Striatum

GRIM-19 was very strongly expressed in the olfactory tubercle, strongly in the caudoputamen (Fig. 3e), and moderately in the nucleus accumbens. Weak staining was observed in the lateral septal nucleus.

Pallidum

Moderate staining was seen throughout the pallidum such as the substantia innominate, medial septal nucleus, diagonal band nucleus, and bed nucleus of the stria terminalis. Meanwhile, weak immunoreactivity was observed in the globus pallidus (Fig. 3f).

Thalamus

In this region, GRIM-19 was expressed at moderate to strong levels (Fig. 4a, b). Specifically, in the paraventricular nucleus, reticular nucleus, nucleus of reuniens, lateral habenula, and mediodorsal nucleus, moderate staining was observed. Strong staining was shown in the anteroventral nucleus, medial habenula, lateral dorsal nucleus, ventral posterior nucleus, lateral geniculate complex, and medial geniculate complex. Very strong immunoreactivity was demonstrated in the anterodorsal nucleus of the thalamus.

Hypothalamus

Weak to moderate staining was observed in most subregions of the hypothalamus (Fig. 4c, d). GRIM-19 was weakly present in the lateral hypothalamic area and moderately in the retrochiasmatic area, dorsomedial hypothalamic nucleus, and ventromedial hypothalamic nucleus. The subfornical organ, suprachiasmatic nucleus, and arcuate nucleus showed extremely strong immunoreactivity.

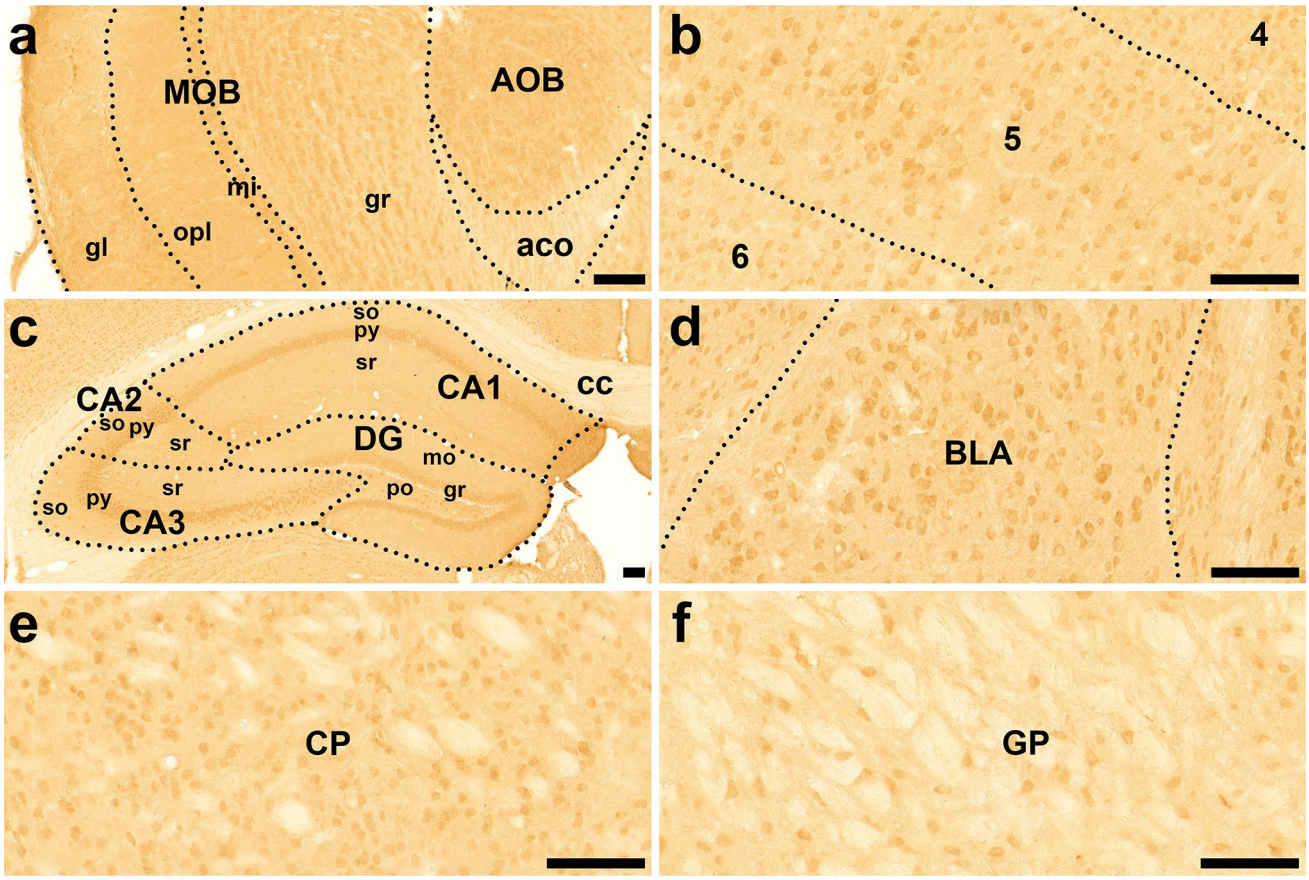

Fig. 3 GRIM-19 immunostaining in the cerebrum. **a** the olfactory bulb. **b** the primary somatosensory cortex. **c** the hippocampus. **d** the amygdala. **e** the caudoputamen. **f** the globus pallidus. *MOB* main olfactory bulb, *AOB* accessory olfactory bulb, *gl* glomerular layer, *opl* outer plexiform layer, *mi* mitral layer, *gr* granule layer, *aco* anterior commissure, *4* internal granular layer, *5* internal pyramidal layer, *6* multiform layer, *CA1* Ammon's horn CA1 subfield, *CA2* Ammon's horn CA2 subfield, *CA3* Ammon's horn CA3 subfield, *DG* dentate gyrus, *so* stratum oriens, *py* pyramidal layer, *sr* stratum radiatum, *mo* molecular layer, *po* polymorph layer, *cc* corpus callosum, *BLA* basolateral amygdalar nucleus, *CP* caudoputamen, *GP* globus pallidus. *Scale bars* indicate 100 μm

Midbrain

Mostly weak staining was detected in the midbrain, such as the superior colliculus, midbrain reticular nucleus, central linear nucleus raphe, and inferior colliculus (Fig. 5a, b). The substantia nigra, both the reticular part (SNr) and the compact part (SNc), exhibited moderate expression.

Pons

Weak to moderate GRIM-19 expression was shown in the pons (Fig. 5c, d). Specifically, the superior central nucleus raphe, pontine reticular nucleus, tegmental reticular nucleus, pontine gray, superior olivary complex, and parabrachial nucleus showed weak immunoreactivity. GRIM-19 immunoreactivity was moderately detected in the nucleus of the lateral lemniscus, principle sensory nucleus of the trigeminal, and motor nucleus of the trigeminal.

Medulla

Overall, weak immunoreactivity was shown in the medulla such as the nucleus prepositus, medial vestibular nucleus, gigantocellular reticular nucleus, parvicellular reticular nucleus, spinal nucleus of the trigeminal, and paragigantocellular reticular nucleus (Fig. 6a, b). Meanwhile, GRIM-19 immunoreactivity was moderately present in the dorsal cochlear nucleus and strongly detected in the ventral cochlear nucleus.

Cerebellum

The molecular and granular layers of the cerebellar cortex showed moderate immunoreactivity, while the Purkinje cell layer exhibited a very strong expression pattern (Fig. 6c, d). Meanwhile, the cerebellar nuclei were weakly stained with GRIM-19 antibody.

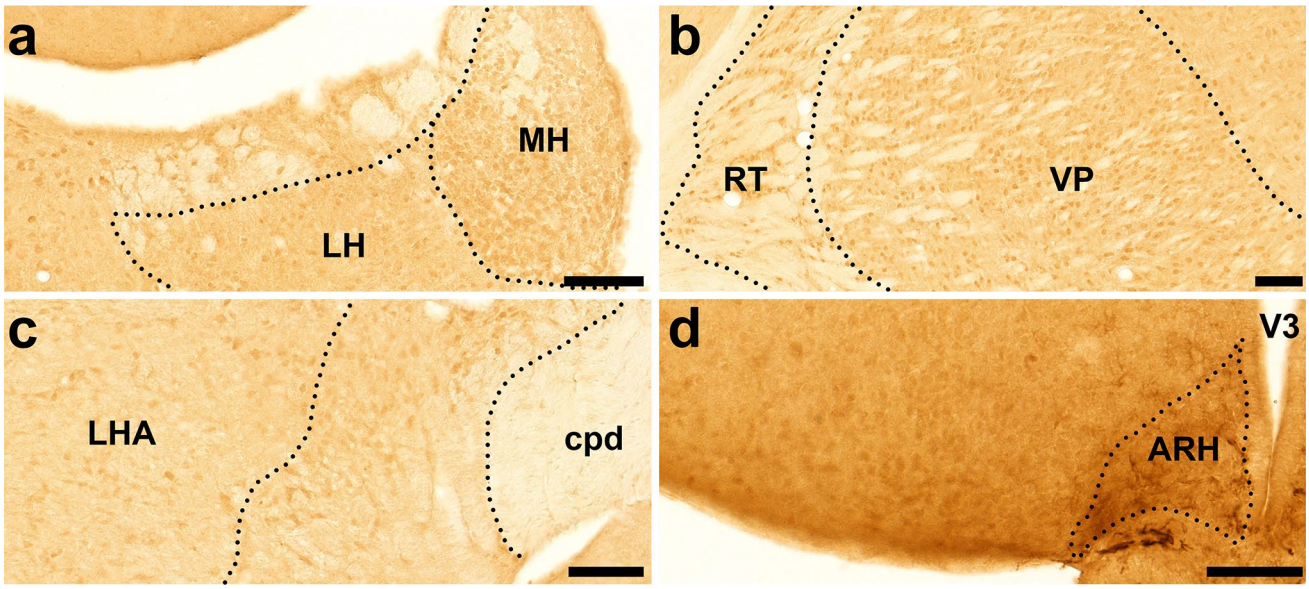

Fig. 4 GRIM-19 immunostaining in the thalamus (**a**, **b**) and hypothalamus (**c**, **d**). *MH* medial habenula, *LH* lateral habenula, *RT* reticular nucleus of the thalamus, *VP* ventral posterior complex of the thalamus, *LHA* lateral hypothalamic area, *cpd* cerebral peduncle, *V3* third ventricle, *ARH* arcuate hypothalamic nucleus. *Scale bars* indicate 100 µm

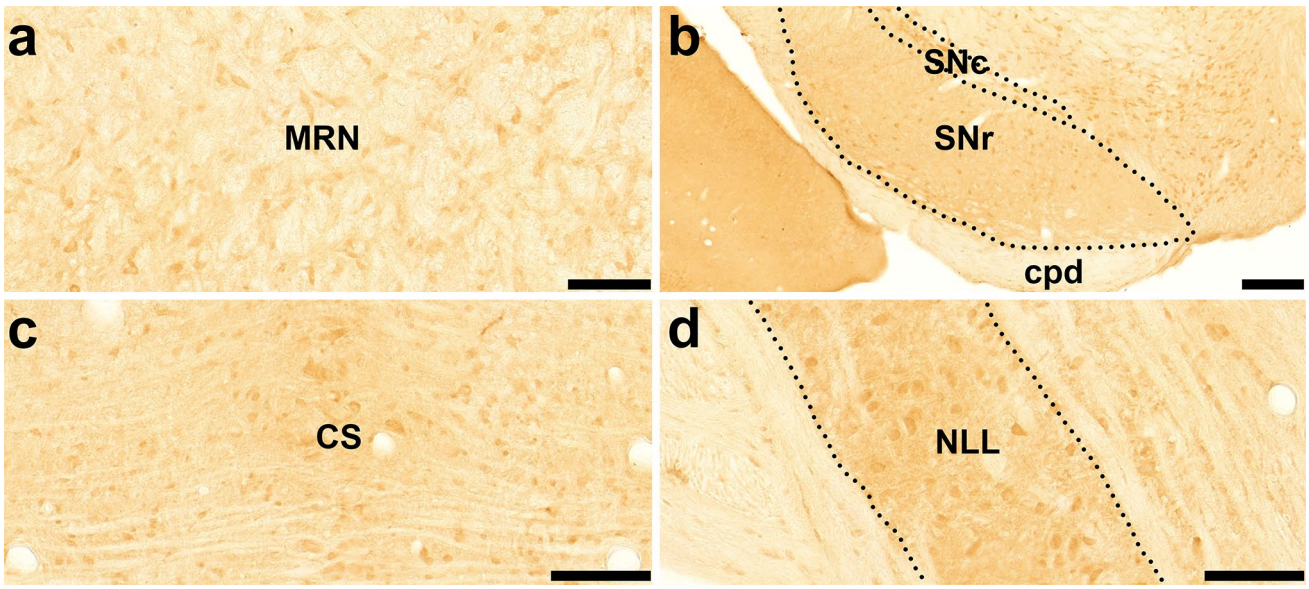

Fig. 5 GRIM-19 immunostaining in the midbrain (**a**, **b**) and pons (**c**, **d**). *MRN* midbrain reticular nucleus, *SNc* substantia nigra compact part, *SNr* substantia nigra reticular part, *cpd* cerebral peduncle, *CS* superior central nucleus raphe, *NLL* nucleus of the lateral lemniscus. *Scale bars* indicate 100 µm

Fiber Tracts

Overall, no staining was observed in the fiber tracts such as the anterior commissure (Fig. 3a), anterior forceps, corpus callosum (Fig. 3c), stria medullaris, internal capsule, cerebral peduncle (Fig. 4c), optic tract, dorsal hippocampal commissure, or arbor vitae (Fig. 6d). The fimbria showed very weak immunoreactivity.

Cell type-Specific Distribution of GRIM-19

To identify the property of neural cells expressing GRIM-19 under normal conditions, double immunofluorescence labeling was performed using antibodies against NeuN, GFAP, Iba1, and OSP to differentiate neurons, astrocytes, microglia, and oligodendrocytes, respectively. Colocalization showed that GRIM-19 was predominantly present in neurons (Fig. 7a–d, q), but not astrocytes (Fig. 7e–h, q), microglia (Fig. 7i–l, q), or oligodendrocytes (Fig. 7m–p, q) under physiological conditions.

Changes in GRIM-19 Expression Pattern Following Transient Global Cerebral Ischemia

To examine the cell type expressing GRIM-19 in the adult mouse hippocampus after transient global cerebral ischemia, double immunofluorescence labeling was performed in the hippocampal CA1 subregion of sham-operated mice (Fig. 8a–d, i–l, q–t, y) and mice subjected to BCCAO followed by 3 days of reperfusion (Fig. 8e–h, m–p, u–x, y). In sham-operated animals, GRIM-19-positive cells were mainly observed in CA1 pyramidal neurons (Fig. 8a–d, y), but not in GFAP- (Fig. 8i–l, y) and Iba1-positive cells (Fig. 8q–t, y). After 3 days of reperfusion following 40 min BCCAO, neuronal cell death (Fig. 8f), reactive astrocytes (Fig. 8n), and microglia (Fig. 8v) were observed in the hippocampal CA1 subregion. At that time, GRIM-19 immunoreactivity was markedly reduced in the CA1 pyramidal cell layer where neuronal cell death occurred (Fig. 8e–h, y).

Fig. 7 Identification of cell types expressing GRIM-19 in the dentate gyrus of the hippocampus. GRIM-19 was merged with the neuronal marker NeuN (**a**–**d**). GRIM-19 was not co-localized with the astrocyte marker GFAP (**e**–**h**), microglia marker Iba1 (**i**–**l**), or oligodendrocyte marker OSP (**m**–**p**). *Scale bar* indicates 125 µm. The plot shows co-labeling rates of GRIM-19 expression in neurons, astrocytes, microglia, or oligodendrocytes (**q**). Data were analyzed by one-way ANOVA and expressed as mean ± SEM based on the results of three mice. *, $P < 0.05$ vs NeuN

However, GRIM-19-expressing cells turned out to be reactive astrocytes (Fig. 8m–p, y) and microglia (Fig. 8u–x, y) in the stratum oriens and stratum radiatum of the hippocampus after BCCAO.

GRIM-19 Expression in the Hippocampal Subgranular Zone

Interestingly, we found that GRIM-19 immunoreactivity was barely detectable in the hippocampal SGZ, in contrast to the granular cell layer that showed strong expression (Fig. 9). We thus suggest that GRIM-19 is expressed only at the late stages of adult neurogenesis because the SGZ is one of the brain regions where adult neurogenesis occurs and contains neural stem and progenitor cells (NSPC), which are expressed at the early stages of adult neurogenesis. To prove this hypothesis, we performed double immunofluorescence staining with stage-specific adult neurogenesis markers: GFAP (radial glial-like neural stem cells marker (type 1)), Ki-67 (type 1, 2, and neuroblast marker (type 3)), DCX (type

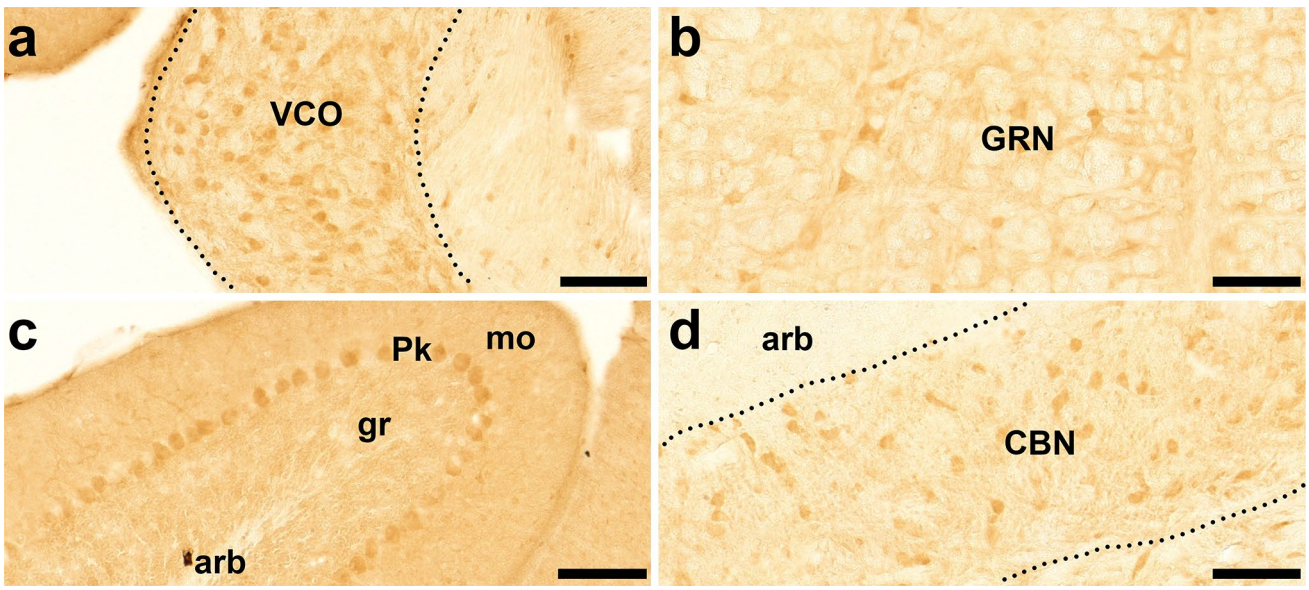

Fig. 6 GRIM-19 immunostaining in the medulla (**a, b**) and cerebellum (**c**, **d**). *VCO* ventral cochlear nucleus, *GRN* gigantocellular reticular nucleus, *mo* molecular layer, *Pk* Purkinje cell layer, *gr* granular layer, *arb* arbor vitae, *CBN* cerebellar nuclei. *Scale bars* indicate 100 µm

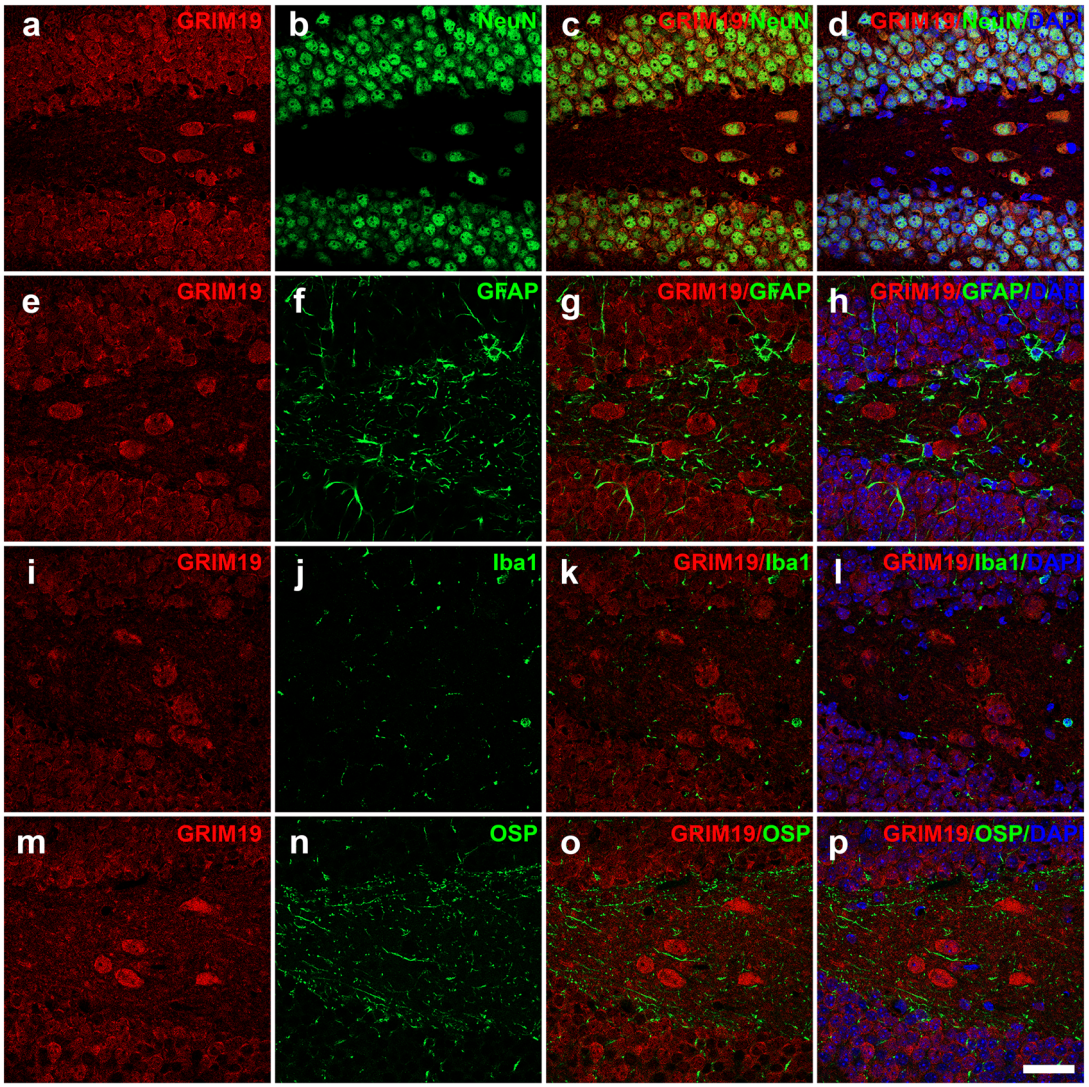
a
GRIM19
b
NeuN
c
GRIM19/NeuN
d
GRIM19/NeuN/DAPI
e
GRIM19
f
GFAP
g
GRIM19/GFAP
h
GRIM19/GFAP/DAPI
i
GRIM19
j
Iba1
k
GRIM19/Iba1
l
GRIM19/Iba1/DAPI
m
GRIM19
n
OSP
o
GRIM19/OSP
p
GRIM19/OSP/DAPI

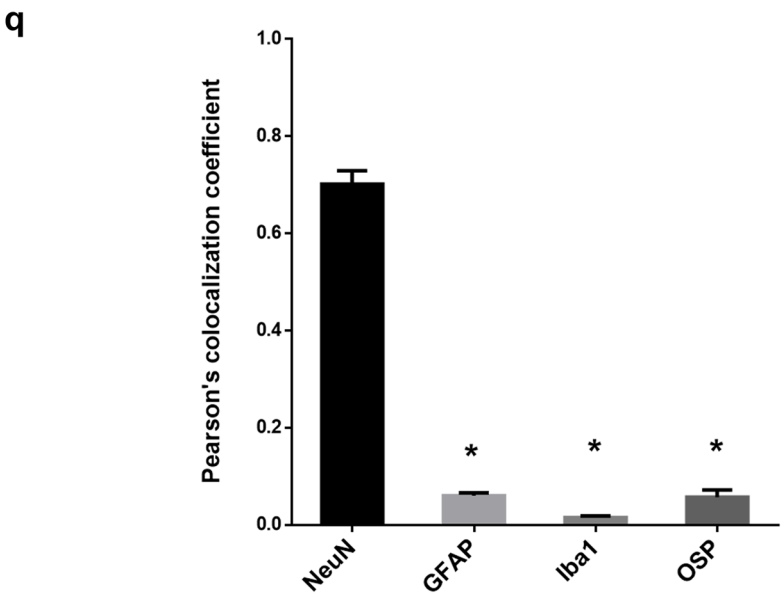
q
Pearson's colocalization coefficient
1.0
0.8
0.6
0.4
0.2
0.0
*
*
*
NeuN
GFAP
Iba1
OSP

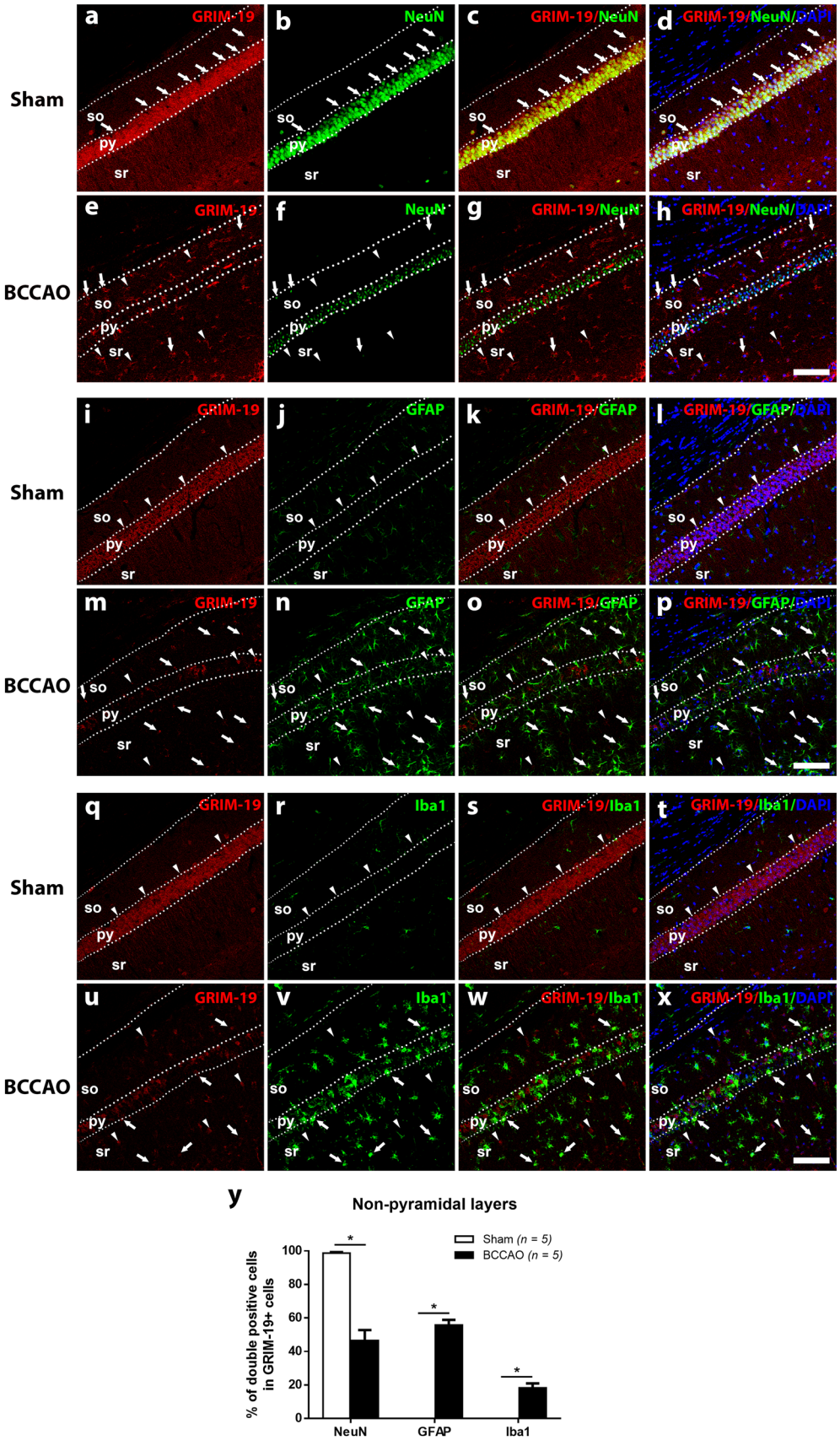
Sham
BCCAO
a GRIM-19
b NeuN
c GRIM-19/NeuN
d GRIM-19/NeuN/DAPI
e GRIM-19
f NeuN
g GRIM-19/NeuN
h GRIM-19/NeuN/DAPI
i GRIM-19
j GFAP
k GRIM-19/GFAP
l GRIM-19/GFAP/DAPI
m GRIM-19
n GFAP
o GRIM-19/GFAP
p GRIM-19/GFAP/DAPI
q GRIM-19
r Iba1
s GRIM-19/Iba1
t GRIM-19/Iba1/DAPI
u GRIM-19
v Iba1
w GRIM-19/Iba1
x GRIM-19/Iba1/DAPI
so
py
sr
y
Non-pyramidal layers
Sham (n = 5)
BCCAO (n = 5)
% of double positive cells in GRIM-19+ cells
100
80
60
40
20
0
*
NeuN
GFAP
Iba1

◂**Fig. 8** Double immunofluorescence staining for GRIM-19 with NeuN (**a**–**h**), GFAP (**i**–**p**), or Iba1 (**q**–**x**) immunostaining in the hippocampal CA1 subregion of sham-operated animals (**a**-**d**, **i**–**l**, **q**–**t**) and mice subjected to BCCAO followed by 3 days of reperfusion (**e**–**h**, **m**–**p**, **u**–**x**). *Arrows* and *arrowheads* indicate examples of double-labeled cells and the cells expressing only GRIM-19, respectively. The graph indicates the ratio of the double-labeled cells to the total GRIM-19-positive cells in the stratum oriens and stratum radiatum of the CA1 subregion (**y**). Data were analyzed by unpaired Student's *t* test and expressed as mean ± S.E.M. *, $P < 0.05$ vs corresponding sham-operated mice. *so* stratum oriens, *sr* stratum radiatum, *py* pyramidal cell layer. *Scale bar* indicates 250 μm

2, 3, and immature granule cell marker), Prox1 (type 2, 3, and immature and mature granule cell marker), PSA-NCAM (type 3 and an immature granule cell marker), Calretinin (an immature granule cell marker), NeuN (an immature and mature granule cell marker), and Calbindin (a mature granule cell marker). GRIM-19 was weakly expressed in GFAP-, Ki-67-, DCX-, and PSA-NCAM-positive cells, but was co-labeled in Prox1-, Calretinin-, NeuN-, and Calbindin-positive cells (Fig. 10). These results indicate that GRIM-19 was not expressed at the early neurogenesis stages, but at the later stages with immature and mature granule cells.

Discussion

In the present study, we demonstrated that GRIM-19 proteins are widely distributed throughout the whole adult mouse brain. This result was expected because GRIM-19 is an indispensable component of the mitochondria (Huang et al. 2004). Our results are supported by regional mRNA expression data from the Allen Brain Atlas (http://mouse.brain-map.org/gene/show/43027), illustrating that GRIM-19 immunoreactivity was ubiquitously expressed throughout the adult mouse brain. In addition, the staining patterns of GRIM-19 in the cortex and hippocampus in the present study are consistent with those provided by Tatarkova et al. (2016). In the present study, double immunofluorescence staining showed that GRIM-19 was co-labeled with NeuN-positive cells but not GFAP-, Iba-1-, or OSP-positive cells, indicating that GRIM-19 is present in neurons rather than astrocytes, microglia, or oligodendrocytes under physiological conditions. On the contrary, an in vitro study showed that GRIM-19 is expressed in the mitochondria from primary cultures of rat cortical astrocytes by Western blot analyses (Mehrabian et al. 2007). This conflicting evidence regarding the presence of GRIM-19 in astrocytes under normal physiological conditions is probably due to the differences between in vitro and in vivo experimental systems. In terms of physiological conditions, an in vivo study is generally regarded as more reliable than an in vitro assay because isolated in vitro culture conditions are highly controlled artificial environments that may not be able to accurately reflect the natural environment of a living organism. Specifically, because in vitro experimental systems use cells grown on a two-dimensional plastic or glass plate (Antoni et al. 2015), the in vitro environment is less physiologically relevant than the in vivo one. The abundant and widespread neuronal distribution of GRIM-19 under physiological conditions suggests that GRIM-19 might play significant roles in the physiological function of the mature brain.

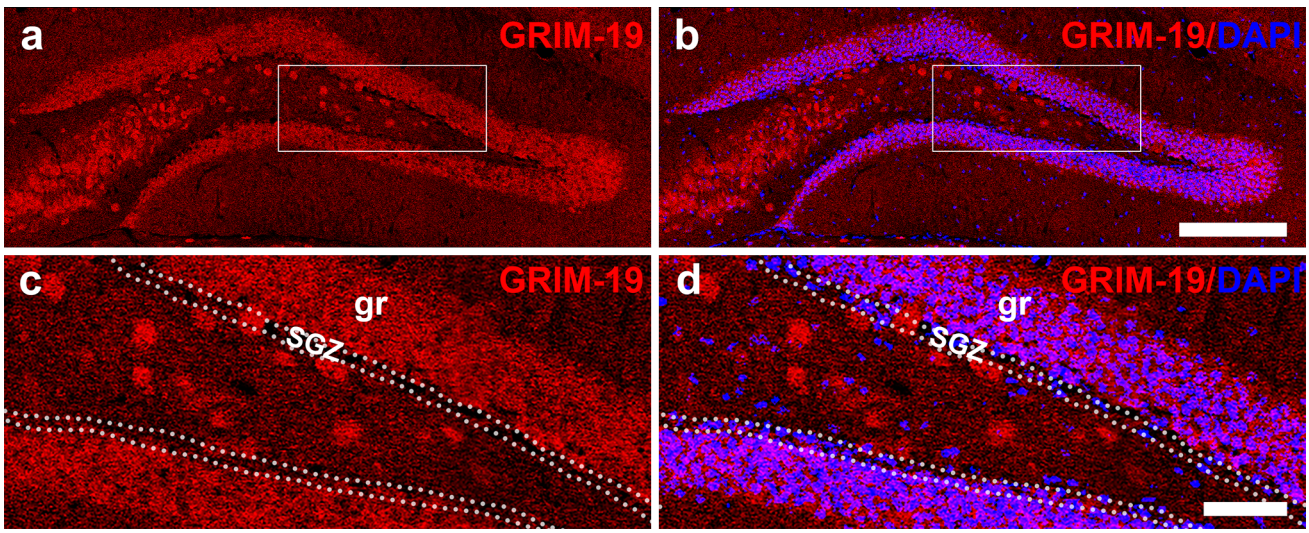

Fig. 9 Weak GRIM-19 immunostaining in the hippocampal subgranular zone. (**c**) and (**d**) are high-magnification views of the boxed areas in (**a**) and (**b**), respectively. *SGZ* subgranular zone, *gr* granular cell layer. *Scale bar* in **b** indicates 200 μm, valid for **a**. *Scale bar* in **d** indicates 50 μm, valid for **c**

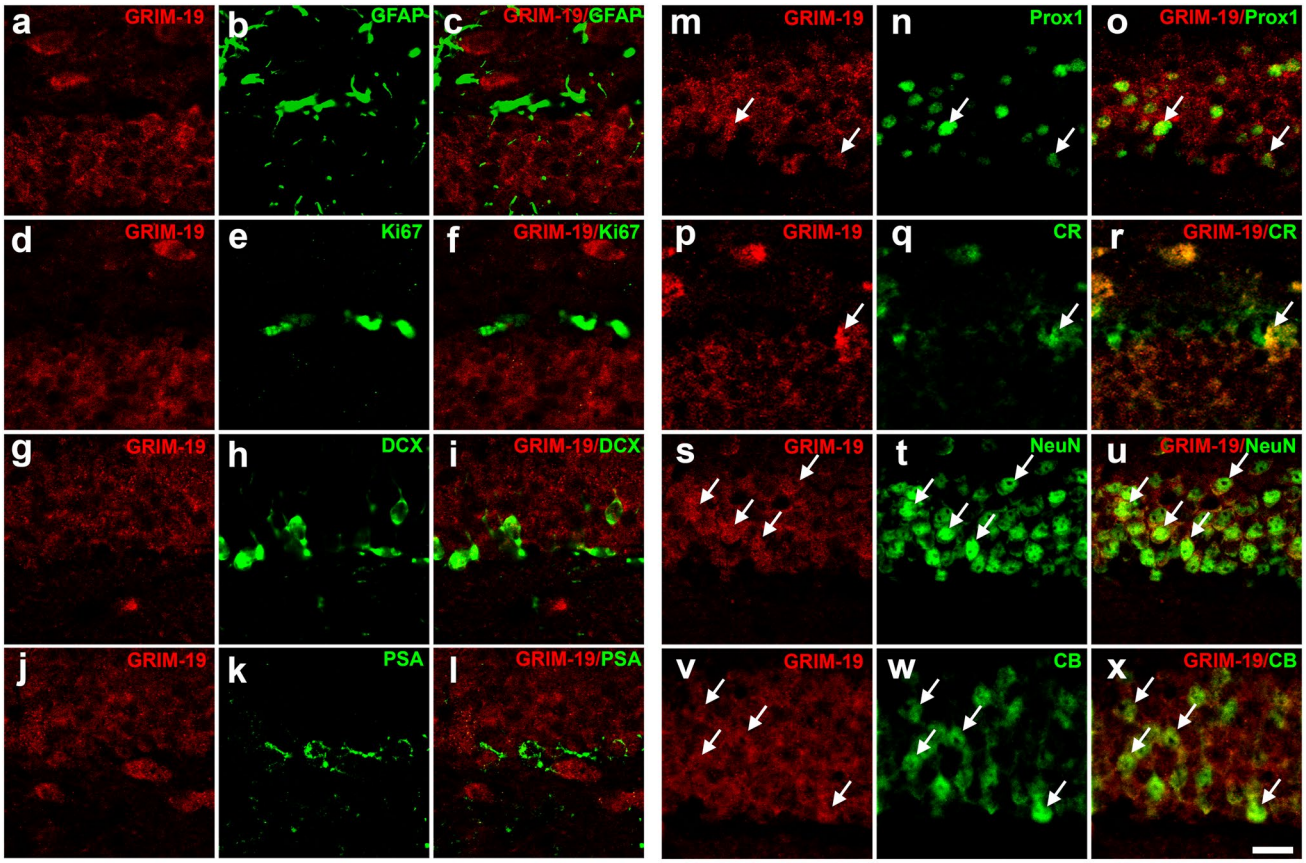

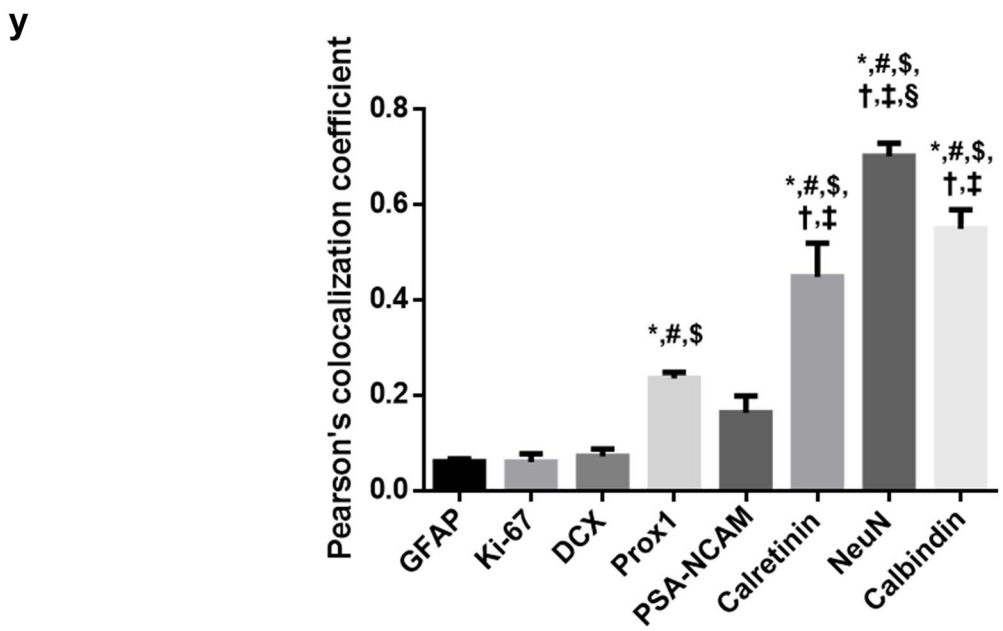

Fig. 10 Double immunofluorescence staining of GRIM-19 with stage-specific adult neurogenesis markers in the hippocampal subgranular zone. GRIM-19 was weakly expressed in GFAP (**a**–**c**)-, Ki-67 (**d**–**f**)-, DCX (**g**–**i**)-, and PSA-NCAM (**j**–**l**)-positive cells but was co-labeled in Prox1(**m**–**o**)-, Calretinin (**p**–**r**)-, NeuN (**s**–**u**)-, and Calbindin (**v**–**x**)-positive cells. *Arrows* indicate examples of double-labeled cells. The plot shows co-labeling rates of GRIM-19 expression with stage-specific adult neurogenesis markers (**y**). Data were analyzed by one-way ANOVA and expressed as mean ± SEM based on the results of three mice. *, $P < 0.05$ vs GFAP; #, $P < 0.05$ vs Ki-67; $, $P < 0.05$ vs DCX; †, $P < 0.05$ vs Prox1; ‡, $P < 0.05$ vs PSA-NCAM; §, $P < 0.05$ vs Calretinin. *PSA* PSA-NCAM, *CR* Calretinin, *CB* Calbindin. *Scale bar* indicates 50 µm

GRIM-19 was first known as a nuclear protein whose expression was induced by apoptotic stimuli in tumor cells (Angell et al. 2000). After discovering that GRIM-19 is a subunit of mitochondrial complex I (Fearnley et al. 2001), many scientists agree that GRIM-19 is predominantly located in mitochondria (Lufei et al. 2003; Huang et al. 2004; Nallar et al. 2010; Chao et al. 2015) and plays a crucial role in both ATP production (Huang et al. 2004; Lu and Cao 2008) and recruitment of STAT3 to the mitochondria (Lufei et al. 2003; Zhang et al. 2003). However, there is still controversy regarding whether GRIM-19 is present in the nucleus or cytosol. Some researchers suggested that GRIM-19 was not detectable in the nucleus or cytosol (Huang et al. 2004; Wegrzyn et al. 2009). Meanwhile, other research groups have shown a trace amount of GRIM-19 in nuclear and/or cytosolic fractions in various cells (Zhang et al. 2004; Nallar et al. 2010). The discrepancies among various studies are likely due to the differences in cell types examined, immunoassay methods employed such as Western blotting and immunofluorescence staining, and the sensitivity of antibodies used. Since there is a continuing debate about the existence of nuclear and/or cytosolic GRIM-19, further investigation is needed using more accurate methods. Our ongoing study is currently investigating intracellular localization of GRIM-19 in adult mouse brain tissues using transmission electron microscope techniques, which have not yet been used to the best of our knowledge.

The present immunohistochemical study revealed that GRIM-19 was not uniformly but site-specifically expressed in the normal mouse brain. These observations may facilitate the study on the pathophysiological roles of GRIM-19 in the brain subregions. For example, we observed very strong immunoreactivity of GRIM-19 in the hippocampus, especially in the pyramidal cell layers and dentate granular cell layer. Considerable evidence indicates that the hippocampus is vulnerable under conditions of increased oxidative stress, such as aging (Geinisman et al. 1995). Indeed, there is a report that lower GRIM-19 protein level was observed in old compared to young rat hippocampus tissue, suggesting that age-related decline of GRIM-19 might be involved in neuronal vulnerability related to oxidative stress (Tatarkova et al. 2016). As another example, there is evidence that the expression of GRIM-19 is significantly decreased in the substantia nigra neurons of Parkinson's patients (Grünewald et al. 2016). This is probably because the reduced levels of GRIM-19 are a consequence of loss of complex I assembly, a common and widely reported phenotype observed in Parkinson's disease (Schapira et al. 1989; Grünewald et al. 2016; Fløngs et al. 2018). In addition, NDUFB8, another complex I subunit, has also been shown to be depleted in postmortem brain tissue of Parkinson's disease (Grünewald et al. 2016; Fløngs et al. 2018). Based on these reports, it is possible that GRIM-19 could be used as one of the pathological hallmarks for Parkinson's disease.

Brain ischemia is the leading cause of death and disability in developed countries (Tong et al. 2016). ROS overproduction after ischemic insult has been considered as a major cause of ischemia/reperfusion injury (Chan 2001). Because GRIM-19 is a composition of the mitochondrial complex I, where ROS are predominantly produced (Kushnareva et al. 2002) and GRIM-19 affects ROS levels (Chen et al. 2012; Hu et al. 2017; Yang et al. 2018), interest in investigating the relationship between GRIM-19 and brain ischemia has grown. Indeed, regarding brain ischemic insult, three different research groups (Schneider et al. 2004; Mehrabian et al. 2007; Chomova et al. 2012) have reported upregulated GRIM-19 expression in affected brain areas. However, overall, we found reduced levels of GRIM-19 in the hippocampal CA1 region of mice subjected to 40 min transient global cerebral ischemia followed by 3 days of reperfusion. This controversial result may be attributed to various reasons, including strain and species differences, the use of different animal models to induce ischemia, differences in the duration of ischemia and reperfusion, and the different assay methods used to quantify GRIM-19 expression levels. Meanwhile, it is noteworthy that scattered GRIM-19-positive cells in the non-pyramidal cell layer of the hippocampus induced by ischemia/reperfusion injury were identified as a portion of reactive astrocytes and microglia. These results raised the possibility that GRIM-19 may play a role in reactive astrocytes and/or microglia following transient global cerebral ischemia.

Intriguingly, our experimental results show that few GRIM-19-positive cells were detected in NSPC in the SGZ, but they were abundant in immature and mature neuronal cells in the granular cell layer. NSPC, which are expressed at the early stages of adult neurogenesis, show high proliferative activity and adopt aerobic glycolysis for metabolism (Zheng et al. 2016; Almeida and Vieira 2017). Similar to NSPC, aerobic glycolysis and high proliferative activity are also key hallmarks of cancer cells (Hsu and Sabatini 2008). Moreover, many scientists have shown that GRIM-19 mRNA and protein expression levels are downregulated in various malignant tumors compared to normal tissues (Máximo et al. 2005; Alchanati et al. 2006; Li et al. 2012), implying an inverse correlation between expression of GRIM-19 and cell proliferation. Furthermore, there is evidence that downregulation of GRIM-19 in tumor cells not only causes metabolic reprogramming from oxidative phosphorylation to aerobic glycolysis (Liu et al. 2013), but also an inability to prevent STAT3-mediated proliferation activity (Zhang et al. 2003). Taken together, these data suggest that GRIM-19 may be implicated in adult neurogenesis in the SGZ, probably through controlling the proliferation and differentiation of

NSPC. Further studies are needed to validate this hypothesis using transgenic or knockout mouse models.

In summary, the present study provided evidence for the immunohistochemical distribution of GRIM-19 in the adult mouse brain. GRIM-19 was widely and heterogeneously distributed throughout the brain. Double immunofluorescence staining revealed that the GRIM-19-positive cells are neurons but not astrocytes, microglia, or oligodendrocytes under normal conditions, implying its substantial involvement in the physiological activity of neurons. Meanwhile, GRIM-19 immunoreactivity was induced in reactive astrocytes and microglia in the hippocampus following transient global cerebral ischemia. Lastly, we presented a new perspective on the relationship between GRIM-19 expression and stemness activity, suggesting that GRIM-19 may control the metabolic programming or proliferation of NSPC. These results can be used as a reference for studying the physiological and pathophysiological roles of GRIM-19 in the adult mouse brain.

Acknowledgements This work was supported by the National Research Foundation of Korea (NRF) Grant NRF-2017R1A2B4002704.

Author Contributions Sun-Nyoung Hwang, Jae-Cheon Kim, and Seong Yun Kim conceived and designed the experiments. Sun-Nyoung Hwang and Jae-Cheon Kim performed experiments and analyzed the data. Seong Yun Kim contributed reagents/materials, interpreted the results, and supervised the project. Sun-Nyoung Hwang and Seong Yun Kim wrote the manuscript. All authors read and approved the final manuscript.

Compliance with Ethical Standards

Conflict of interest The authors declare that they have no conflict of interest.

Ethical Approval All animal procedures were approved by the Ethics Committee of the Catholic University of Korea and were performed in accordance with the National Institutes of Health's Guide for the Care and Use of Laboratory Animals (NIH Publication No. 80-23). This article does not contain any studies with human participants performed by any of the authors.

References

Alchanati I, Nallar SC, Sun P, Gao L, Hu J, Stein A, Yakirevich E, Konforty D, Alroy I, Zhao X, Reddy SP, Resnick MB, Kalvakolanu DV (2006) A proteomic analysis reveals the loss of expression of the cell death regulatory gene GRIM-19 in human renal cell carcinomas. Oncogene 25(54):7138–7147. https://doi.org/10.1038/sj.onc.1209708

Almeida AS, Vieira HLA (2017) Role of cell metabolism and mitochondrial function during adult neurogenesis. Neurochem Res 42(6):1787–1794. https://doi.org/10.1007/s11064-016-2150-3

Angell JE, Lindner DJ, Shapiro PS, Hofmann ER, Kalvakolanu DV (2000) Identification of GRIM-19, a novel cell death-regulatory gene induced by the interferon-beta and retinoic acid combination, using a genetic approach. J Biol Chem 275(43):33416–33426. https://doi.org/10.1074/jbc.M003929200

Antoni D, Burckel H, Josset E, Noel G (2015) Three-dimensional cell culture: a breakthrough in vivo. Int J Mol Sci 16(3):5517–5527. https://doi.org/10.3390/ijms16035517

Chan PH (2001) Reactive oxygen radicals in signaling and damage in the ischemic brain. J Cereb Blood Flow Metab 21(1):2–14. https://doi.org/10.1097/00004647-200101000-00002

Chao L, Wang X, Yang Y, Cui W, Xu J, Chen H, Hao A, Deng X (2015) Downregulation of gene expression and activity of GRIM-19 affects mouse oocyte viability, maturation, embryo development and implantation. J Assist Reprod Genet 32(3):461–470. https://doi.org/10.1007/s10815-014-0413-y

Chen Y, Lu H, Liu Q, Huang G, Lim CP, Zhang L, Hao A, Cao X (2012) Function of GRIM-19, a mitochondrial respiratory chain complex I protein, in innate immunity. J Biol Chem 287(32):27227–27235. https://doi.org/10.1074/jbc.M112.340315

Cho KO, Kim SK, Cho YJ, Sung KW, Kim SY (2007) Regional differences in the neuroprotective effect of minocycline in a mouse model of global forebrain ischemia. Life Sci 80(22):2030–2035. https://doi.org/10.1016/j.lfs.2007.03.005

Choi YS, Cho KO, Kim EJ, Sung KW, Kim SY (2007) Ischemic preconditioning in the rat hippocampus increases antioxidant activities but does not affect the level of hydroxyl radicals during subsequent severe ischemia. Exp Mol Med 39(4):556–563. https://doi.org/10.1038/emm.2007.61

Chomova M, Tatarkova Z, Dobrota D, Racay P (2012) Ischemia-induced inhibition of mitochondrial complex I in rat brain: effect of permeabilization method and electron acceptor. Neurochem Res 37(5):965–976. https://doi.org/10.1007/s11064-011-0689-6

Fearnley IM, Carroll J, Shannon RJ, Runswick MJ, Walker JE, Hirst J (2001) GRIM-19, a cell death regulatory gene product, is a subunit of bovine mitochondrial NADH:ubiquinone oxidoreductase (complex I). J Biol Chem 276(42):38345–38348. https://doi.org/10.1074/jbc.C100444200

Fløynes IH, Fernandez-Vizarra E, Lykouri M, Brakedal B, Skeie GO, Miletic H, Lilleng PK, Alves G, Tysnes OB, Haugarvoll K, Dölle C, Zeviani M, Tzoulis C (2018) Neuronal complex I deficiency occurs throughout the Parkinson's disease brain, but is not associated with neurodegeneration or mitochondrial DNA damage. Acta Neuropathol 135(3):409–425. https://doi.org/10.1007/s00401-017-1794-7

Geinisman Y, Detoledo-Morrell L, Morrell F, Heller RE (1995) Hippocampal markers of age-related memory dysfunction: behavioral, electrophysiological and morphological perspectives. Prog Neurobiol 45(3):223–252. https://doi.org/10.1016/0301-0082(94)00047-L

Grünewald A, Rygiel KA, Hepplewhite PD, Morris CM, Picard M, Turnbull DM (2016) Mitochondrial DNA depletion in respiratory chain-deficient Parkinson disease neurons. Ann Neurol 79(3):366–378. https://doi.org/10.1002/ana.24571

Halliwell B (1989) Oxidants and the central nervous system: some fundamental questions. Acta Neurol Scand 80(s126):23–33. https://doi.org/10.1111/j.1600-0404.1989.tb01779.x

Hsu PP, Sabatini DM (2008) Cancer cell metabolism: warburg and beyond. Cell 134(5):703–707. https://doi.org/10.1016/j.cell.2008.08.021

Hu H, Nan J, Sun Y, Zhu D, Xiao C, Wang Y, Zhu L, Wu Y, Zhao J, Wu R, Chen J, Yu H, Hu X, Zhu W, Wang J (2017) Electron leak from NDUFA13 within mitochondrial complex I attenuates ischemia-reperfusion injury via dimerized STAT3. Proc Natl Acad Sci USA 114(45):11908–11913. https://doi.org/10.1073/pnas.1704723114

Huang G, Lu H, Hao A, Ng DC, Ponniah S, Guo K, Lufei C, Zeng Q, Cao X (2004) GRIM-19, a cell death regulatory protein, is essential for assembly and function of mitochondrial complex I. Mol Cell Biol 24(19):8447–8456. https://doi.org/10.1128/MCB.24.19.8447-8456.2004

Kalakonda S, Nallar SC, Jaber S, Keay SK, Rorke E, Munivenkatappa R, Lindner DJ, Fiskum GM, Kalvakolanu DV (2013) Monoallelic loss of tumor suppressor GRIM-19 promotes tumorigenesis in mice. Proc Natl Acad Sci USA 110(45):E4213–E4222. https://doi.org/10.1073/pnas.1303760110

Kushnareva Y, Murphy AN, Andreyev A (2002) Complex I-mediated reactive oxygen species generation: modulation by cytochrome c and NAD(P)$^+$oxidation-reduction state. Biochem J 368(2):545–553. https://doi.org/10.1042/BJ20021121

Lee JM, Grabb MC, Zipfel GJ, Choi DW (2000) Brain tissue responses to ischemia. J Clin Invest 106(6):723–731. https://doi.org/10.1172/JCI11003

Li F, Ren W, Zhao Y, Fu Z, Ji Y, Zhu Y, Qin C (2012) Downregulation of GRIM-19 is associated with hyperactivation of p-STAT3 in hepatocellular carcinoma. Med Oncol 29(5):3046–3054. https://doi.org/10.1007/s12032-012-0234-8

Liu Q, Wang L, Wang Z, Yang Y, Tian J, Liu G, Guan D, Cao X, Zhang Y, Hao A (2013) GRIM-19 opposes reprogramming of glioblastoma cell metabolism via HIF1α destabilization. Carcinogenesis 34(8):1728–1736. https://doi.org/10.1093/carcin/bgt125

Lu H, Cao X (2008) GRIM-19 is essential for maintenance of mitochondrial membrane potential. Mol Biol Cell 19(5):1893–1902. https://doi.org/10.1091/mbc.e07-07-0683

Lufei C, Ma J, Huang G, Zhang T, Novotny-Diermayr V, Ong CT, Cao X (2003) GRIM-19, a death-regulatory gene product, suppresses Stat3 activity via functional interaction. EMBO J 22(6):1325–1335. https://doi.org/10.1093/emboj/cdg135

Mattson MP, Duan W, Pedersen WA, Culmsee C (2001) Neurodegenerative disorders and ischemic brain diseases. Apoptosis 6(1–2):69–81. https://doi.org/10.1023/A:1009676112184

Máximo V, Botelho T, Capela J, Soares P, Lima J, Taveira A, Amaro T, Barbosa AP, Preto A, Harach HR, Williams D, Sobrinho-Simões M (2005) Somatic and germline mutation in GRIM-19, a dual function gene involved in mitochondrial metabolism and cell death, is linked to mitochondrion-rich (Hürthle cell) tumours of the thyroid. Br J Cancer 92(10):1892–1898. https://doi.org/10.1038/sj.bjc.6602547

Mehrabian Z, Chandrasekaran K, Kalakonda S, Kristian T, Fiskum G, Kalvakolanu DV (2007) The IFN-beta and retinoic acid-induced cell death regulator GRIM-19 is upregulated during focal cerebral ischemia. J Interferon Cytokine Res 27(5):383–392. https://doi.org/10.1089/jir.2006.0067

Nallar SC, Kalakonda S, Sun P, Ohmori Y, Hiroi M, Mori K, Lindner DJ, Kalvakolanu DV (2010) Identification of a structural motif in the tumor-suppressive protein GRIM-19 required for its antitumor activity. Am J Pathol 177(2):896–907. https://doi.org/10.2353/ajpath.2010.091280

Okamoto T, Inozume T, Mitsui H, Kanzaki M, Harada K, Shibagaki N, Shimada S (2010) Overexpression of GRIM-19 in cancer cells suppresses STAT3-mediated signal transduction and cancer growth. Mol Cancer Ther 9(8):2333–2343. https://doi.org/10.1158/1535-7163.MCT-09-1147

Rizzardi AE, Johnson AT, Vogel RI, Pambuccian SE, Henriksen J, Skubitz AP, Metzger GJ, Schmechel SC (2012) Quantitative comparison of immunohistochemical staining measured by digital image analysis versus pathologist visual scoring. Diagn Pathol 7:42. https://doi.org/10.1186/1746-1596-7-42

Schapira AH, Cooper JM, Dexter D, Jenner P, Clark JB, Marsden CD (1989) Mitochondrial complex I deficiency in Parkinson's disease. Lancet 333(8649):1269. https://doi.org/10.1016/S0140-6736(89)92366-0

Schneider A, Laage R, von Ahsen O, Fischer A, Rossner M, Scheek S, Grünewald S, Kuner R, Weber D, Krüger C, Klaussner B, Götz B, Hiemisch H, Newrzella D, Martin-Villalba A, Bach A, Schwaninger M (2004) Identification of regulated genes during permanent focal cerebral ischaemia: characterization of the protein kinase 9b5/MARKL1/MARK4. J Neurochem 88(5):1114–1126. https://doi.org/10.1046/j.1471-4159.2003.02228.x

Tatarkova Z, Kovalska M, Timkova V, Racay P, Lehotsky J, Kaplan P (2016) The effect of aging on mitochondrial complex I and the extent of oxidative stress in the rat brain cortex. Neurochem Res 41(8):2160–2172. https://doi.org/10.1007/s11064-016-1931-z

Tong JT, Eyngorn I, Mlynash M, Albers GW, Hirsch KG (2016) Functional neurologic outcomes change over the first 6 months after cardiac arrest. Crit Care Med 44(12):e1202–e1207. https://doi.org/10.1097/CCM.0000000000001963

Varghese F, Bukhari AB, Malhotra R, De A (2014) IHC Profiler: an open source plugin for the quantitative evaluation and automated scoring of immunohistochemistry images of human tissue samples. PLoS ONE 9(5):e96801. https://doi.org/10.1371/journal.pone.0096801

Wegrzyn J, Potla R, Chwae YJ, Sepuri NB, Zhang Q, Koeck T, Derecka M, Szczepanek K, Szelag M, Gornicka A, Moh A, Moghaddas S, Chen Q, Bobbili S, Cichy J, Dulak J, Baker DP, Wolfman A, Stuehr D, Hassan MO, Fu XY, Avadhani N, Drake JI, Fawcett P, Lesnefsky EJ, Larner AC (2009) Function of mitochondrial Stat3 in cellular respiration. Science 323(5915):793–797. https://doi.org/10.1126/science.1164551

Yang Y, Cheng L, Deng X, Yu H, Chao L (2018) Expression of GRIM-19 in unexplained recurrent spontaneous abortion and possible pathogenesis. Mol Hum Reprod 24(7):366–374. https://doi.org/10.1093/molehr/gay020

Zhang J, Yang J, Roy SK, Tininini S, Hu J, Bromberg JF, Poli V, Stark GR, Kalvakolanu DV (2003) The cell death regulator GRIM-19 is an inhibitor of signal transducer and activator of transcription 3. Proc Natl Acad Sci USA 100(16):9342–9347. https://doi.org/10.1073/pnas.1633516100

Zhang X, Huang Q, Yang Z, Li Y, Li CY (2004) GW112, a novel antiapoptotic protein that promotes tumor growth. Cancer Res 64(7):2474–2481. https://doi.org/10.1158/0008-5472.CAN-03-3443

Zheng X, Boyer L, Jin M, Mertens J, Kim Y, Ma L, Ma L, Hamm M, Gage FH, Hunter T (2016) Metabolic reprogramming during neuronal differentiation from aerobic glycolysis to neuronal oxidative phosphorylation. Elife 5:e13374. https://doi.org/10.7554/eLife.13374